(Received 1 January 2024, Accepted 22 February 2024, Scheduled 29 February 2024)

High Gain Compact Dual Band Antenna Using Frequency Selective Surface for 5G and WLAN Applications

Shubhangi Verulkar[1], Anjali Rochkari[2], Mahadu Trimukhe[2], Varsha Bodade[2], and Rajiv Gupta[2,*]

[1] K. C. College of Engineering and Management Studies and Research, Thane, India
[2] Terna Engineering College, Navi-Mumbai, India

ABSTRACT: In this paper, a high gain antenna using Frequency Selective Surface (FSS) is proposed. The compact structure is designed from a circular Ultra-wideband (UWB) monopole. Higher order modes of UWB antenna are suppressed by decreasing the thickness of the monopole, ground plane dimensions, and increasing the gap between the ground plane and the monopole. Symmetrical portion of circular monopole is etched to form a semicircular monopole, and an off-set feed is employed. Dual band characteristics and miniaturization are achieved by etching horizontal and vertical slots and reducing ground plane dimensions. An FSS reflector is designed for gain enhancement. This miniaturized antenna offers less blockage and therefore, higher gain improvement when an FSS is used as a reflector.

1. INTRODUCTION

5G and 6G technology offer seamless connectivity. Reliable access with high data rate and low latency has made virtual business using augmented reality a part of our life. Significant bearing on economy has motivated researchers to improve performance and functionality of 5G technology and deploy 5G networks. It has provided an impetus to the design of novel antenna for 5G applications.

Microstrip antenna is very popular in wireless communication applications, considering its various features like simple design, ease of fabrication, light weight, and planar configuration. It can offer linear and circular polarizations and can operate over single or multi-band. However, it has narrow bandwidth and low gain [1]. Monopole antennas offer wide bandwidth but omnidirectional radiation pattern with peak gain about 0–2 dBi. Multi-band monopole antennas are reported in literature. Compact multi-band antennas enhance the functionality, reduce the cost, and improve the performance of the system.

Multi-branches multi-band monopole antennas are designed [1–3]. Slots are etched in radiating patch and ground plane [4–7] to achieve multi-band characteristics. Fractal techniques are also employed to achieve multi-band operation [8, 9]. Dual band split ring monopole antennas structures operating over the sub 6 GHz 5G bands have been reported [10]. However, in many cases, we require wide band and multi-band directional antennas.

Planar reflectors or reflective layers are employed to enhance the gain of antenna. Artificial Magnetic Conductor (AMC), High Impedance Surface (HIS), FSS or meta material surfaces are designed to improve the antenna gain [11–20]. An FSS based slotted semicircular UWB antenna is proposed. Peak gain of 8.3 dBi over 3 to 12 GHz is achieved [11]. A fork shaped monopole antenna with 3×3 array of HIS is designed to improve the gain of monopole. 7.34 dBi peak gain at 3 GHz is achieved [12]. A slot shaped antenna with modified circular loop FSS is reported. Peak gain of 7.9 dBi over 3.6 to 6.1 GHz is achieved [13]. An AMC reflector is used to improve the gain of a dual band split ring monopole antenna. Peak gains of 5 dBi and 7.5 dBi over 2.37–2.5 GHz and 4.45–4.9 GHz respectively are achieved [14].

A dual band U-shaped antenna with a meander line stub is proposed. An FSS consisting of an array of square loop shaped unit cell is employed. Peak gains of 6.8 dBi and 9.0 dBi are achieved over 2.3–2.65 GHz and 4.9–6.45 GHz, respectively [15]. Gain enhancement techniques using FSS are discussed in [16]. Single or multi-layer FSS is used as a reflector for obtaining directional radiation characteristics over UWB frequencies. A super-wideband antenna with two inverted U-shaped and a flower shaped slots in radiator is designed to operate over 3.1–15 GHz. The peak gain of 8.3 dBi over UWB is achieved by using a 3×3 array of I-shaped split ring meta material unit cell as a superstrate at $\lambda/3$ height [17]. Four different layers of FSS reflector, each with different periodicity is employed. A star shaped patch antenna with a step feedline is designed, and a square patch is etched in ground plane. The peak gain of 7–8 dBi over 3 to 11.7 GHz is obtained [18].

A tri-band rectangle-shaped antenna using inverted U- and L-shaped slots is designed. Gain of the antenna is enhanced by 3.58 dBi using AMC [19]. A circle-shaped UWB monopole antenna with FSS as a reflector at a height of $\lambda/4$ is designed. The peak gain of 9.7 dBi over 3.1 to 6.0 GHz is obtained. Overall antenna dimensions with FSS are $108 \times 108 \times 20\,\text{mm}^3$ [20]. Using a planar corner reflector, the gain of antenna is improved from 2.2 to 6.4 dBi over 3.1 to 10.6 GHz. Dimensions of antenna with reflector are $20 \times 20 \times 15\,\text{mm}^3$ [21]. A UWB high gain antenna is designed using a curved single layer FSS, and the peak gain of 12 dBi over 2.66 to 17.98 GHz (148% BW) is

* Corresponding author: Rajiv Gupta (rajivgupta@ternaengg.ac.in).

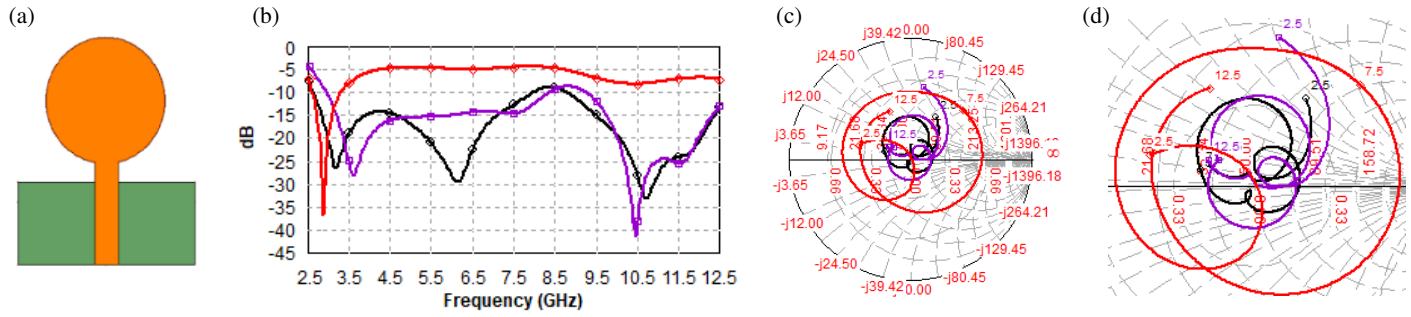

FIGURE 1. (a) Geometry of CMPA, simulated (b) return loss, (c) impedance variation plot, (d) magnified impedance variation plot.

TABLE 1. Optimized parameters of the structure in mm.

W_s	L_s	L_g	W_g	L_f	W_f	R	$L1$	$W1$	$L2$	$W2$	$L3$	$W3$	$W4$	$W5$	t	W
12	22	4.1	10.8	11.2	3	8	1	3.5	1	7	2.86	1	2.5	7.4	2	5.4

achieved. However, the antenna has large curved FSS dimensions of $1.3\lambda_0 \times 1.3\lambda_0$ [22]. A microstrip antenna (MSA) using meta-material for 5G applications [23] and a planar antenna for THz application [24] are designed using an iterative wave design procedure. A novel wide band beam forming antenna array is designed without using phase shifter and crossover. Thus, a switched beam antenna system is introduced in [25].

Here, a dual band antenna for 5G sub-6 GHz applications using FSS as a reflector is designed to improve the gain of the antenna. Antenna gains of 8.0 dBi at 3.45 GHz and 8.3 dBi at 5.25 GHz are achieved, and the gain improvement is 6.3 dBi and 5.8 dBi over lower and upper bands, respectively. Dual band characteristics and miniaturization are achieved by etching the symmetrical portion of circular monopole, offset feed, by etching horizontal and vertical slots and reducing the dimensions of ground plane. This miniaturized antenna offers minimum blockage and therefore, higher gain improvement when FSS is used as reflector.

2. DESIGN THEORY AND ANTENNA GEOMETRY

Electromagnetic coupling between higher order modes that provide ultra-wide bandwidth depends on the shape and thickness of the monopole. A circular monopole offers wider bandwidth than rectangular monopole as higher order modes excited in a circular monopole are combatively close to each other as compared to rectangular monopole. Impedance bandwidth depends on the dimensions and shape of monopole, ground plane dimensions, and the gap between the ground plane and radiating patch. Higher order modes can be suppressed by decreasing the thickness of the monopole, ground plane dimensions, and increasing the gap between the ground plane and the monopole. It mean circular monopole which consists of a circle of radius 10mm.

2.1. Single Element Dual Band Antenna Design

A circular monopole antenna (CMPA), which consists of a circle of radius 10 mm, is designed on a 1.6 mm thick FR4 substrate ($\varepsilon_r = 4.4$, $\tan\delta = 0.02$) using IE3D simulator, shown in Fig. 1. The lowest frequency corresponding to $S_{11} = -9.5$ dB of a circular monopole is given by [27]

$$f_L = 72/((2.25 \times R + g) \times k) \quad (1)$$

where R and g in mm are the radius of circular monopole and the gap between the ground and patch respectively while f_L is in GHz. The value of k is 1.15 for the FR-4 substrate [26, 27]. In CMPA-1 ($R = 10$ mm, $g = 0.3$ mm and ground plane dimensions are 28 mm $\times$ 14 mm), the simulated f_L is 2.62 GHz while the calculated f_L from Equation (1) is 2.74 GHz. The fundamental resonating mode and two higher order modes are observed over 2.5–12.5 GHz. S_{11} minima occur at 3.1, 6.1, and 10.65 GHz. In CMPA-2, as the radius is decreased to 8 mm, the structure resonates in fundamental mode, and only one higher order mode is observed over 2.5–12.5 GHz. S_{11} minima occur at 3.6 and 10.4 GHz. In CMPA-3, 'g' is increased to 6.3 mm, and ground plane dimensions are decreased to 13 mm $\times$ 8 mm. The structure resonates only in fundamental mode ($R = 8$ mm and $g = 6.3$ mm). It resonates at 2.87 GHz and $S_{11} \leq -10$ dB over 2.62–3.26 GHz. S_{11} and impedance variation of these structures are shown in Fig. 1. In CMPA-1, there are three loops on the impedance variation plots around 3.15 GHz, 6.1 GHz, and 10.65 GHz inside the reflection coefficient circle of 0.33, while in CMPA-2 there are only two loops around 3.6 GHz and 10.4 GHz. In CMPA-3, no loop is formed inside reflection coefficient circle of 0.33. It depicts that the higher order modes can be suppressed by decreasing the radius and ground plane dimensions and increasing 'g'. The dual band antenna is evolved using CMPA-3 to operate over 3.3–4.0 GHz and 5.6–6.0 GHz.

The geometry of the dual-band antenna and its detailed dimensions are depicted in Fig. 2 and Table 1, respectively. The step-by-step evolution of antenna is shown in Fig. 3. The dual-band antenna is derived from a CMPA 'Antenna 1'.

Since the CMPA Antenna 1 is symmetrical, half portion is etched, and a semicircular monopole with an off-set feed is designed as Antenna 2. The ground plane dimensions are de-

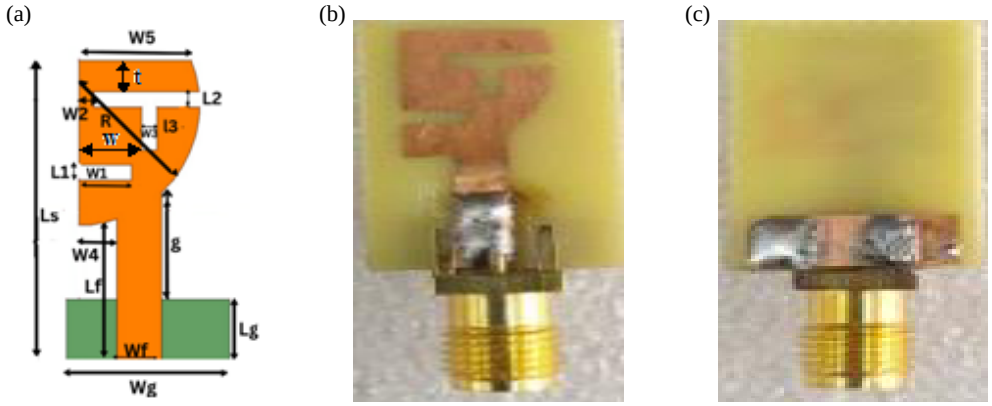

FIGURE 2. (a) Geometry. (b) Top view. (c) Bottom view of fabricated structure.

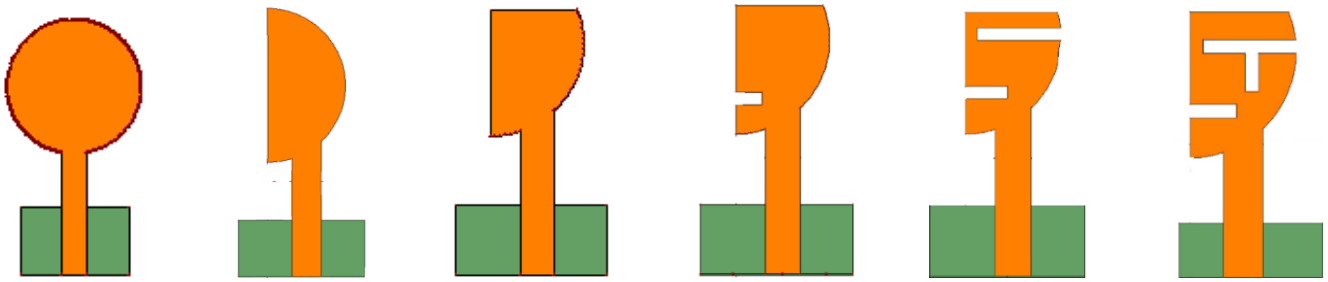

FIGURE 3. Evolution stages of the proposed antenna.

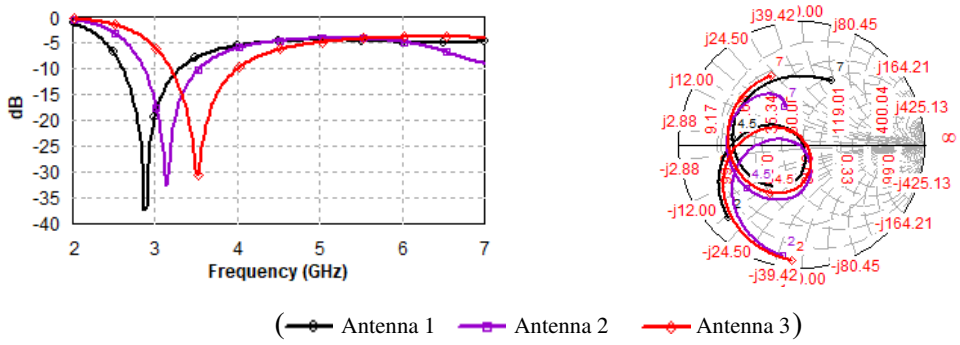

FIGURE 4. Simulated S_{11} and impedance variation.

creased to 13 mm × 6 mm, and 'g' is decreased to 6.0 mm. It resonates at 3.1 GHz with $S_{11} \leq -10$ dB over 2.86–3.56 GHz.

Since there is little current at the center and top of the Antenna 2, in Antenna 3, 5 mm portion from the top of the semicircle is etched to decrease the dimensions of antenna and increase the resonating frequency so that the antenna operates over the desired 3.3–3.6 GHz, 5G band. It resonates at 3.5 GHz with $S_{11} \leq -10$ dB over 3.18–4.0 GHz. S_{11} and impedance variation plot of these structures are shown in Fig. 4. As 'g' is decreased in Antenna 2, the impedance becomes more capacitive, though the decrease in ground plane dimensions decreases the capacitive effect. The decrease in the dimensions of the radiating monopole, in Antenna 3, further decreases the capacitance of the structure as shown in Fig. 4.

In a monopole antenna, the surface current density is mainly concentrated at the edges of a monopole. Therefore, a horizontal slot $S1$ of length $L1$ and width $W1$ is etched at a distance 'g' from the edge of ground plane in Antenna 3 to form Antenna 4. The slot $S1$ increases the capacitance, and thus the resonant frequency decreases with the introduction of slot $S1$. The impedance plot shifts downward due to increase in capacitance. Thus, the slot helps in miniaturization of antenna. Antenna 4 resonates at 3.39 GHz with $S_{11} \leq -10$ dB over 3.1–3.8 GHz. Another slot $S2$ of length $L2$ and width 'R-$W2$' is etched at a distance 't' from the top edge of monopole antenna in Antenna 4, and the structure is termed as Antenna 5. The slot increases the capacitance. As a result, the resonant frequency decreases, and the impedance plot shifts downward. Slot $S2$

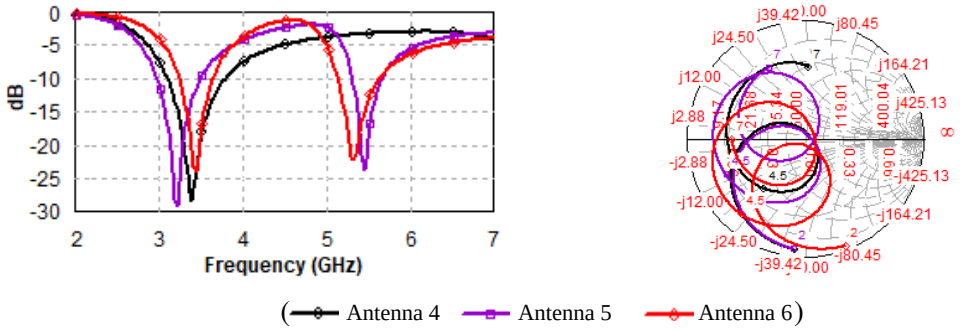

FIGURE 5. Simulated S_{11} and impedance variation.

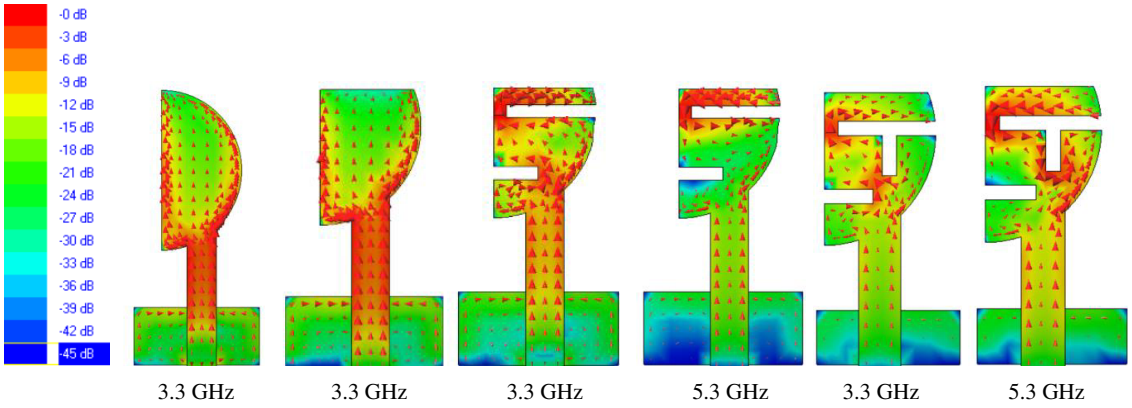

FIGURE 6. Simulated surface current density of Antenna 2, Antenna 3, Antenna 5, and Antenna 6.

also results in two distinct current paths, and thus the structure operates over dual bands. Antenna 5 resonates at 3.22 GHz and 5.4 GHz, and $S_{11} \leq -10$ dB over 2.98–3.5 GHz and 5.32–5.66 GHz as shown in Fig. 5. In Antenna 5, at 3.3 GHz, there is significant surface current density over the entire structure; however, the surface current density is less in the area just below the right of slot $S2$, and the vector surface current density shows that the surface current tends to flow towards the left. At 5.4 GHz, the surface current density is evenly distributed in the area just below the right of slot $S2$, and the vector surface current density shows that the surface current tends to flow towards the right edge. The surface current densities of Antenna 2, Antenna 3, and Antenna 5 at resonant frequencies are shown in Fig. 6.

Now, a vertical slot $S3$ of length $L3$ and width '$W3$' is etched at a distance 'W' from the left edge of monopole antenna towards the right just below the slot $S2$ in Antenna 5 to form Antenna 6. Antenna 6 resonates at 3.3 GHz and 5.3 GHz, and $S_{11} \leq -10$ dB over 3.25–3.65 GHz and 5.14–5.62 GHz (Fig. 5). Since the surface current density, in Antenna 5, in the area just below the slot $S2$ is less, and it tends to flow towards left, slot $S3$ effectively decreases the current path length over the lower band. The scalar and vector current density at 3.4 GHz depicts that significant current flows from the left of slot $S3$ and comparatively quite less current on the right of slot $S3$. Thus, resonant frequency of lower band increases due to decrease in effective current path length. However significant surface current around slot $S3$ increases the effective current path length over the upper band, and therefore, resonant frequency of the upper band decreases. Thus, dimensions of slots $S1$, $S2$, and $S3$ control the dual band operation. The surface current densities of Antenna 2, Antenna 3, and Antenna 5 are depicted in Fig. 6. To analyze the structure, a parametric study is carried out.

The dimensions of slot $S1$ affect the lower band more than the upper band as surface current density is concentrated around $S1$ at lower band. The increase in length of $L1$ decreases the resonant frequency of lower band. Similarly, the resonant frequency of lower band decreases with increase in $W1$. The surface current is mainly concentrated over the left portion of the feed line at lower band and over the right portion of the feed line at upper band. As a result, $L1$ and $W1$ have little effect on upper band. Fig. 7 shows S_{11} for different $L1$ and $W1$.

Since the surface current density around slot $S2$ is significantly more at upper band than at lower band, the dimensions of slot $S2$ affect the upper band more than lower band. The resonant frequencies of both the bands decrease with increase in $L2$. As the electric path length increases more at upper band, the resonant frequency of upper band decreases more than lower band. The increase in $W2$ also decreases the resonant frequencies of both the bands. However, its effect is less than $L2$. The increase in $L2$ increases the perimeter around slot $S2$ more than increase in $W2$. Further, as $W2$ increases the effective current path length increases, which should decrease the resonant frequency, but decrease in capacitance of the slot due to increase

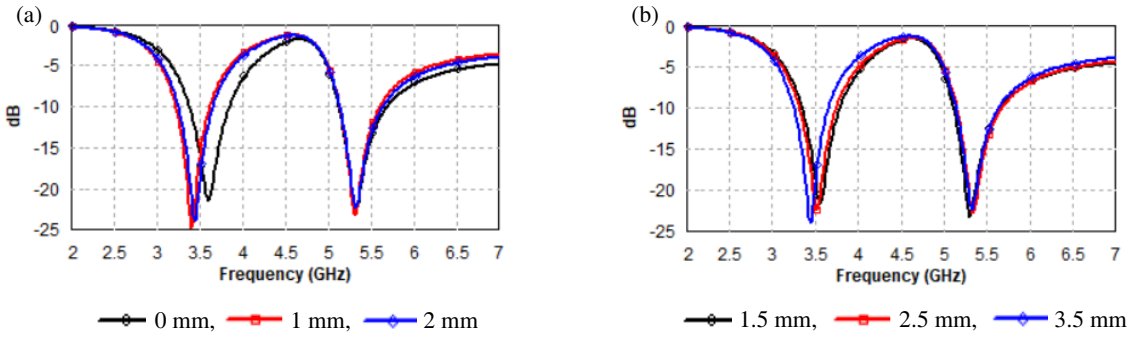

FIGURE 7. Simulated S_{11}, (a) different $L1$, (b) different $W1$.

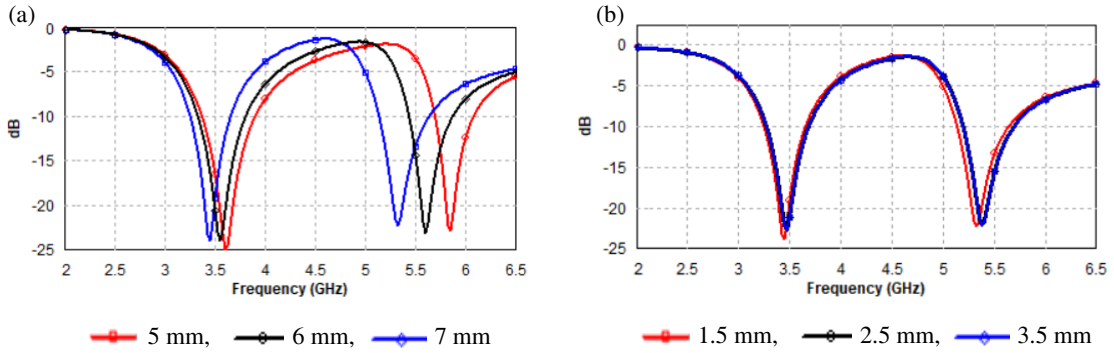

FIGURE 8. Simulated S_{11}, (a) different $L2$, (b) different $W2$.

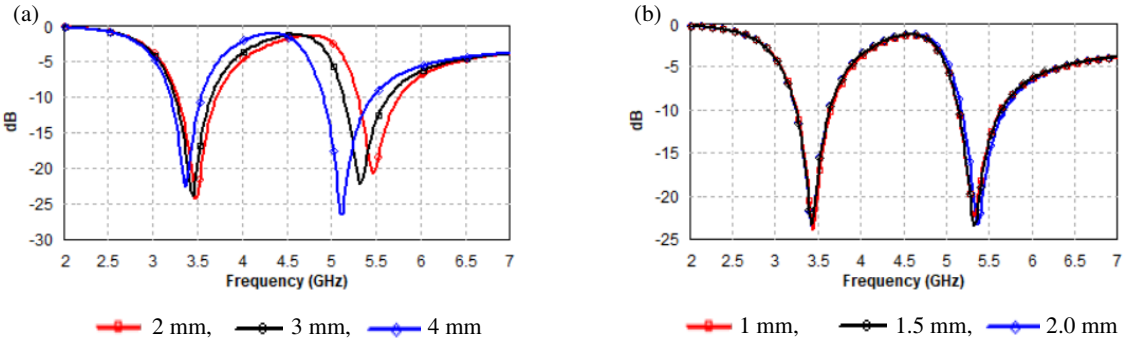

FIGURE 9. Simulated S_{11}, (a) different $L3$, (b) different $W3$.

in $W2$ offsets the decrease in resonant frequency. S_{11} for different $L2$ and $W2$ are shown in Fig. 8.

Since the surface current density around slot $S3$ is significantly more at upper band than at lower band, the dimensions of slot $S3$ affect the upper band more than lower band. The resonant frequencies of both the bands decrease with an increase in $L3$. As the electric path length decreases more at upper band, the resonant frequency of upper band decreases more than lower band. The increase in $W3$ has little effect on resonant frequencies of both the bands. As $W3$ increases the effective current path length increases, and it should decrease the resonant frequency, but decrease in capacitance of the slot due to increase in $W3$ balances out the decrease in resonant frequency. However, its effect is less than $L3$. S_{11} for different $L3$ and $W3$ are shown in Fig. 9.

3. DUAL BAND HIGH GAIN ANTENNA USING FSS

The gain of a monopole antenna can be increased by placing an FSS layer at a height below the monopole antenna. FSS consists of an array of elements or unit cells with fixed inter-element spacing and periodicity. FSS layer reflects the fields radiated by a monopole antenna, and if these fields are in phase with the fields radiated by the monopole in upward direction, it causes constructive interference and results in increase in directivity and gain. The gain of antenna depends on the shape, size, spacing between the unit cell of FSS, dielectric constant and thickness of substrate, and height of FSS from the antenna [12, 13]. The center of FSS layer is aligned to the center of monopole antenna. There is little effect of small misalignment of center of monopole relative to FSS layer on impedance bandwidth and gain of antenna.

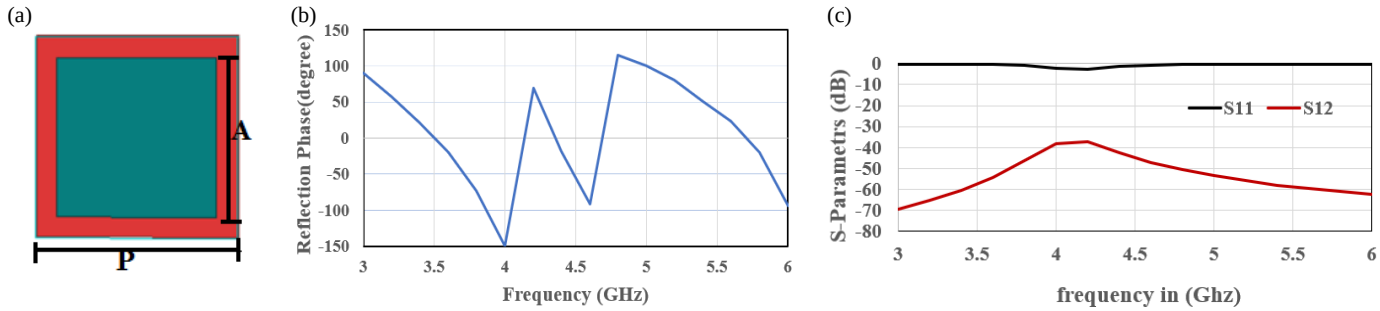

FIGURE 10. (a) FSS unit cell; simulated (b) reflection phase, (c) S-parameters.

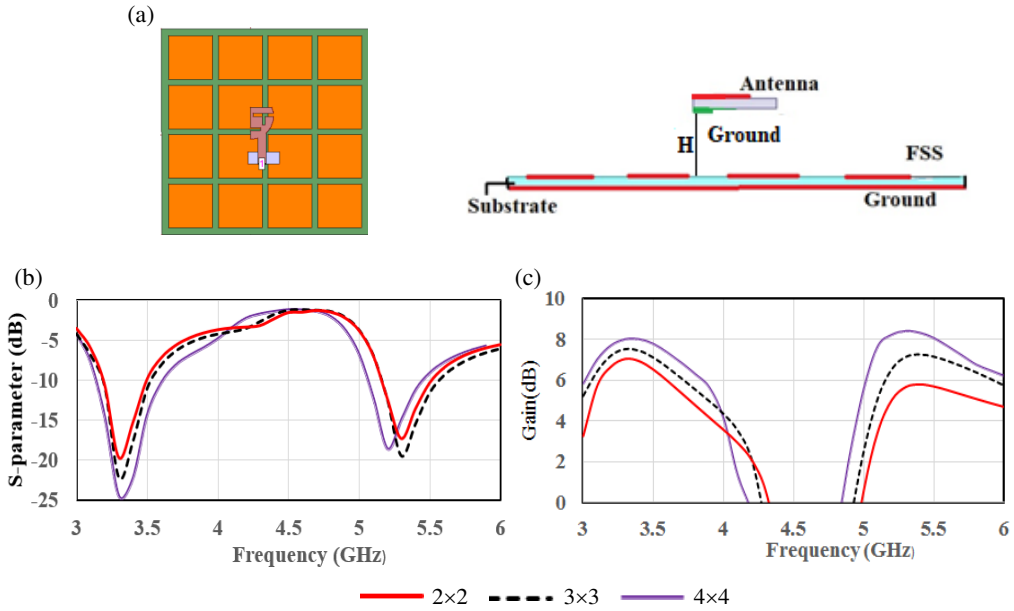

FIGURE 11. (a) Antenna with 4×4 array FSS; Simulated (b) S_{11}, (c) antenna gain for different array size.

3.1. Design of Unit Cell

The magnitude and phase of reflection coefficient of FSS determine the gain of antenna. An FSS consisting of an array of unit cells is designed on a $h = 1.6$ mm thick FR4 substrate. Full-wave Floquet analysis of FSS is carried out on a unit cell, by ANSYS High Frequency Structure Simulator (HFSS), as shown in Fig. 10(a). For constant periodicity, resonant frequency corresponding to 0° reflection phase decreases with the increase in patch dimensions while for constant patch size, it increases with periodicity. Square patch of side $A = 15$ mm and periodicity $P = 17$ mm offers the desired AMC bandwidth (corresponding to $\pm 90°$ phase variation) from 3.2 to 3.7 GHz and 5.15 to 5.5 GHz. The reflection phase in Fig. 10(b) depicts that the reflection phase varies linearly over 3.2–3.7 GHz and 5.15–5.5 GHz. S_{11} and S_{12} plots in Fig. 10(c) depict that FSS reflects the waves as S_{11} is close to 0 dB, and $S_{12} < -40$ dB over the desired bands from 3.2–3.7 GHz and 5.15–5.5 GHz.

The effect of array size or dimensions of FSS, spacing between the antenna and FSS, unit cell patch dimension, and the spacing between the metallic patches of FSS is studied. The effect of shape of metallic patch on antenna gain is also analyzed.

3.2. Effect of Array Size of FSS

The top and side views of the antenna with 4×4 array FSS and S_{11} and gain variation for different array sizes are shown in Fig. 11. FSS increases the gain of antenna as the waves radiated from the monopole antenna are reflected and constructively interfere with the radiated waves in the forward direction. The gain of antenna depends on the dimensions or array size of FSS. As the array size increases, the gain increases, but the improvement in gain decreases with increase in array size. The increase in array size also increases the size of FSS and antenna. FSS dimensions with a 4×4 array of unit cell are $70 \times 70 \times 1.6$ mm^3. It is fabricated on a 1.6 mm thick FR4 substrate and placed at 12 mm from the dual band monopole antenna. FSS dimension or unit cell array size of FSS also affects the impedance matching of antenna. Impedance matching and bandwidth improve with the increase in unit cell array size [11, 13]. Front to back lobe ratio also improves with array size. However, the size of antenna limits the array size of FSS. FSS comprising a 4×4 array of unit cell provides 8.0 dBi and 8.3 dBi peak gains over 3.2–3.7 GHz and 5.15–5.5 GHz.

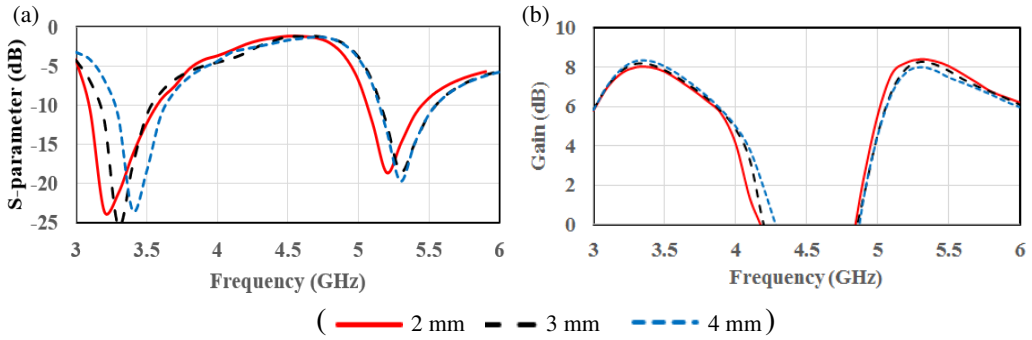

FIGURE 12. Simulated (a) S_{11}, (b) gain variation for different spacing between patches of FSS.

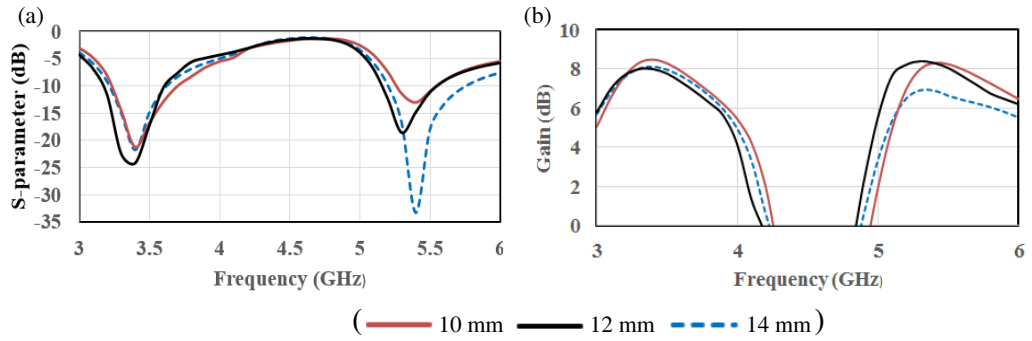

FIGURE 13. Simulated (a) S_{11}, (b) gain for different FSS height.

3.3. Effect of Spacing between Metallic Patches

The edge to edge spacing between the metallic patches of FSS affects the gain of the antenna. As the spacing is increased, the gain decreases. The decrease in gain is more at upper band than at lower band as electrical spacing (S/λ) increases with the increase in frequency. As the capacitance increases, the resonant frequency decreases with decrease in spacing between FSS patches. S_{11} and gain variation for different spacing between the patches of 4×4 array FSS are shown in Fig. 12.

3.4. Effect of FSS Height from Monopole Antenna

FSS increases the gain of antenna as the waves radiated from the monopole antenna are reflected and constructively interfere with the radiated waves in the forward direction. Maximum gain is obtained at a particular height when the fields radiated by a monopole in forward direction interfere constructively with the fields reflected from the FSS. As the height between the monopole and FSS is varied from this optimum height, the maximum gain of the antenna decreases over the desired dual bands. FSS height has little effect at lower band; however, impedance matching improves with the increase in FSS height from antenna over upper band. S_{11} and gain variation for different heights of FSS is shown in Fig. 13.

3.5. Effect of Shape of Metallic Patch of FSS

Effect of shape of metallic patch on the gain of the antenna is also analyzed. FSS comprising an array of square (15 mm side) metallic patch provides higher gain than the array of circle (15 mm diameter) or hexagon (7.5 mm side) shaped metallic patches. The effective metallic area and therefore, reflection magnitude is more for square metallic patch array than circular or hexagonal metallic patch array. Therefore, higher gain is obtained with the FSS comprising square patches. Antenna with FSS comprising different shapes of metallic patches is shown in Fig. 14(a). S_{11} and gain of antenna for these FSS are shown in Fig. 14(b) and Fig. 14(c), respectively.

FSS enhances the gain of antenna if the waves radiated from the monopole antenna and reflected from FSS constructively interfere with the radiated waves in the forward direction. Let ϕt be the phase of fields transmitted by monopole in forward direction, ϕr be the phase of the reflected waves, and ϕs be the phase delay corresponding to the complete propagation trip between monopole and FSS of height H, then for constructive interference Equation (2) should be satisfied.

$$\phi t = \phi s + \phi r \quad \text{and} \quad \phi s = 2 \times 2\Pi \times f \times H/c \qquad (2)$$

Maximum antenna gain is obtained at 12 mm spacing between FSS and antenna over dual bands using 4×4 array FSS layer. The gain variation and antenna efficiency of dual band antenna with and without FSS are shown in Fig. 15. Peak gain with FSS is improved to 8.0 dBi and 8.3 dBi from 1.7 dBi and 2.3 dBi without FSS over 3.2–3.7 GHz and 5.15–5.5 GHz, respectively.

The scalar and vector surface current distributions are shown in Fig. 16. The radiated fields from the monopole antenna illuminate the FSS layer. The central patches of FSS are illuminated more than the patches at the edges. The surface current on the metallic patches is in phase and thus helps in improving gain of the antenna. The horizontal components of surface current give rise to cross polarization.

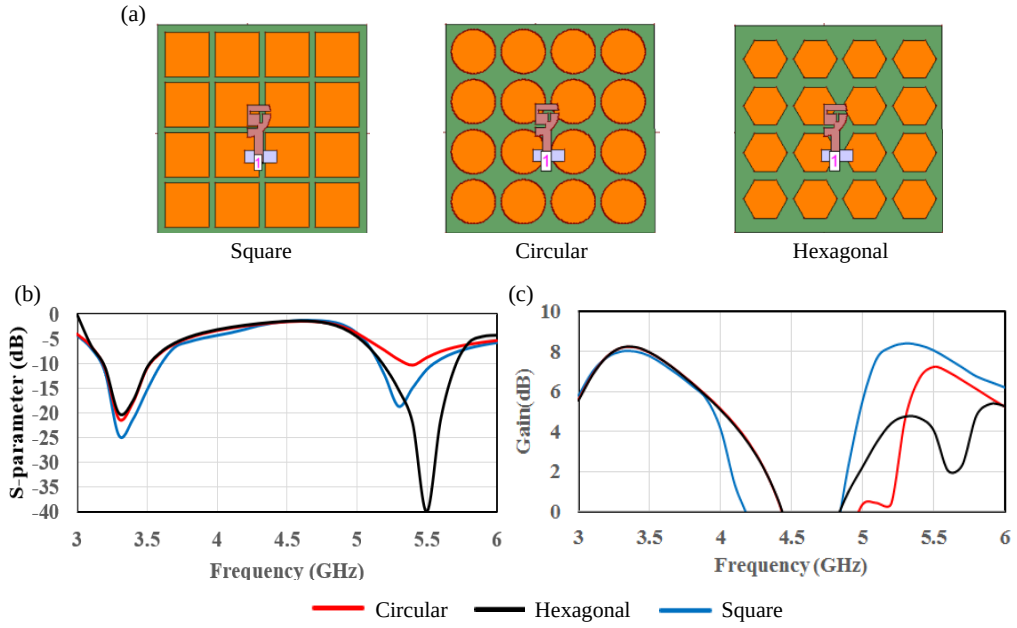

FIGURE 14. (a) FSS comprising of an array of patches of different shape; Simulated (b) S_{11}; (c) Gain variation.

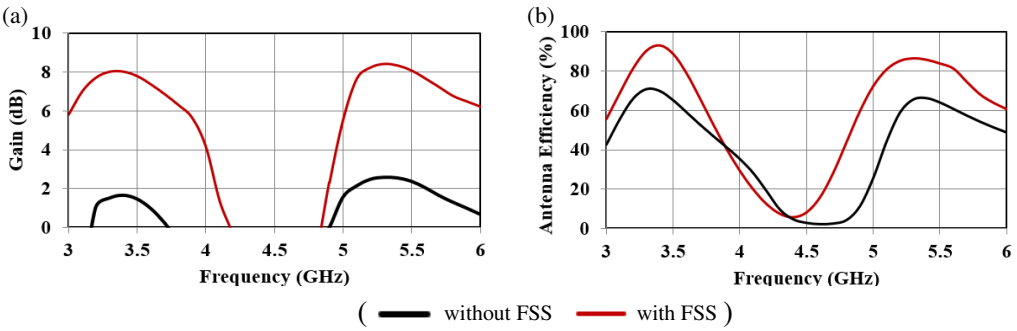

FIGURE 15. Simulated (a) gain; (b) Antenna efficiency.

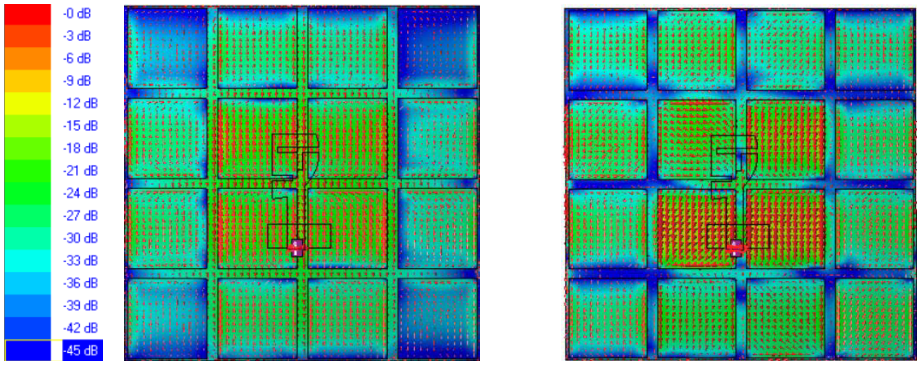

FIGURE 16. Simulated scalar and vector surface current distribution of antenna with FSS.

4. FABRICATION AND MEASURED RESULTS

S-parameters and radiation patterns of the fabricated antenna (Fig. 17) are measured using Agilent 9916A network analyzer and standard horn antenna in an anechoic chamber. Simulated and measured S_{11} parameters and antenna gains are shown in Fig. 18. The compact size of monopole antenna causes less blockage to the fields reflected by FSS, and therefore, the antenna offers higher gain improvement. Gain improvement decreases as dimensions of monopole antenna increase due to blockage. Fig. 19 shows the radiation patterns at 3.45 GHz and 5.25 GHz. The cross polarization is more at 5.25 GHz than at

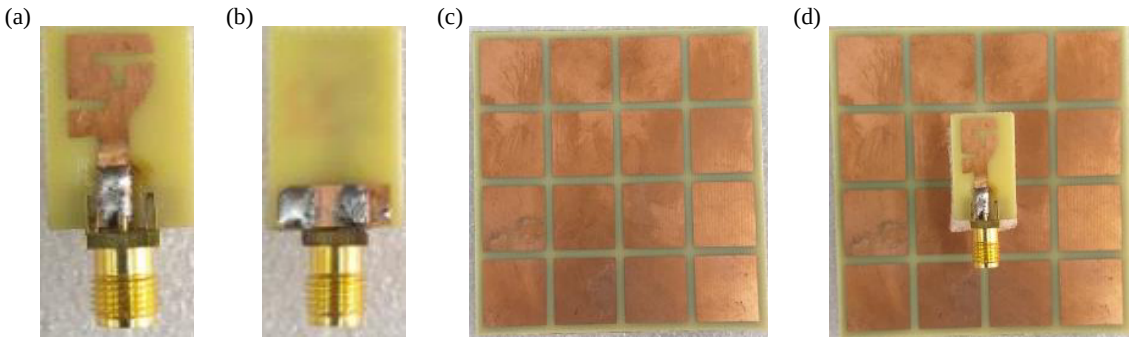

FIGURE 17. (a) Top view, (b) bottom view of monopole antenna, (c) FSS, (d) antenna with FSS.

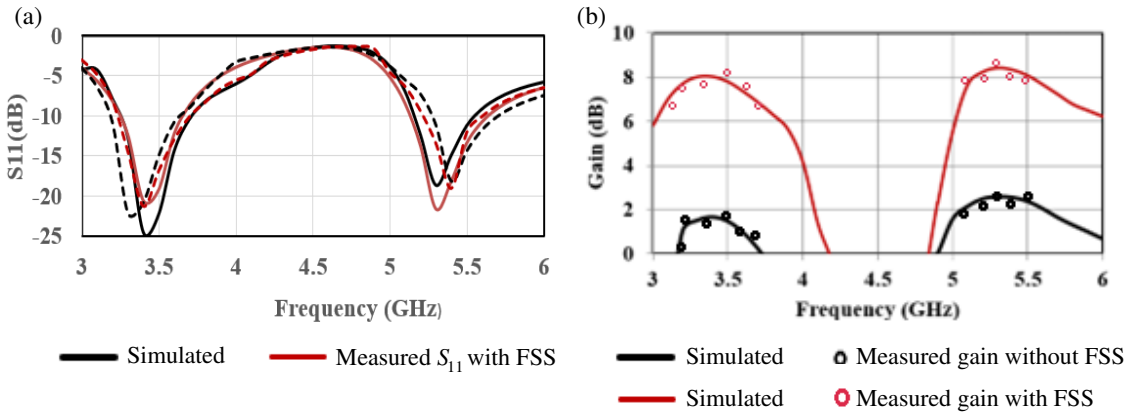

FIGURE 18. (a) Simulated and measured S_{11} with FSS. (b) Simulated and measured gain without FSS.

TABLE 2. Comparison with reported antennas.

Ref.	Monopole Antenna (mm^3)	Antenna with Reflector (mm^3)	Operating Bands GHz	Electrical Size of Antenna with FSS	Peak Gain dBi
[11]	$30 \times 30 \times 1.6$	$62.5 \times 63 \times 25$	3–12	$0.625 \times 0.63 \times 0.25$	8.3
[12]	$60 \times 42 \times 1.57$	$66 \times 66 \times 5.77$	2.7–3.5	$0.59 \times 0.59 \times 0.059$	7.34
[13]	$28 \times 36 \times 1.6$	$79.9 \times 79.9 \times 8$	2.37–2.5 4.45–4.9	$0.63 \times 0.63 \times 0.064$	5 7.5
[19]	$32 \times 28 \times 1.6$	$108 \times 108 \times 20$	3.1–6.0	$1.116 \times 1.116 \times 0.207$	9.7
[21]	$29.2 \times 29.2 \times 1.6$	$79.6 \times 79.6 \times 7$	3.14–3.83 4.40–5.02	$0.833 \times 0.833 \times 0.073$	7.1 8.2
This work	$21 \times 12.8 \times 1.6$	$70 \times 70 \times 12$	3.2–3.7 5.15–5.5	$0.746 \times 0.746 \times 0.128$	8.0 8.3

3.45 GHz due to significant increase in horizontal electric field component at 5.25 GHz.

5. COMPARISON WITH STATE OF ART ANTENNAS

The proposed antenna is compared with reported antennas with respect to dimensions of monopole antenna, overall dimensions of antenna with reflector, operating bands, and peak gain in Table 2. The antenna in [11] is a high-profile antenna. The antenna in [19] offers higher gain but has significant larger dimensions than the proposed antenna. [12] and [13] are smaller in dimensions but offer less gain, whereas [21] has larger lateral dimensions and less gain. The dual band monopole antenna designed to enhance the gain has smaller dimensions than [19, 21] and thus offers minimum blockage and maximum gain improvement. The antenna is simple to design, low in cost, and offers 8.0 dBi peak gain over lower 5G band and 8.3 dBi peak gain over upper WLAN band.

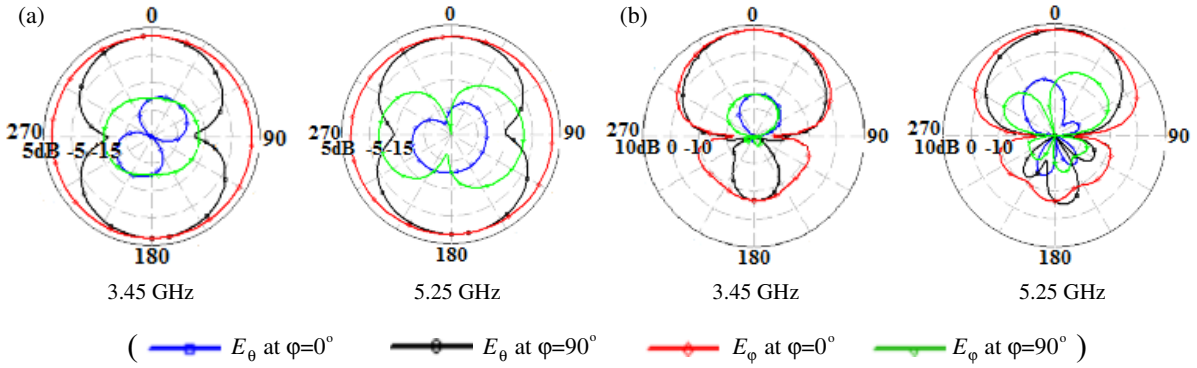

FIGURE 19. Measured radiation patterns, (a) without FSS, (b) with FSS.

6. CONCLUSION

A compact dual band monopole antenna is designed, and antenna gain is enhanced by using an FSS reflector. Due to compact size, the monopole offers less blockage and gain improvement of 6.3 and 5.8 dBi over lower 5G and upper WLAN band, respectively. The antenna is simple to design, small, and low in cost. The optimized structure provides $S_{11} \leq -10$ dB over 3.2–3.7 GHz, 5G and 5.15–5.5 GHz, WLAN bands. The $0.746\lambda_0 \times 0.746\lambda_0 \times 0.128\lambda_0$ prototype antenna offers the peak gain of 8.0 dBi at 3.45 GHz and 8.3 dBi at 5.25 GHz, and the gain improvement is 6.3 and 5.8 dBi over lower and upper bands, respectively. λ_0 is the free-space wavelength at 3.2 GHz. Antenna efficiency is 92.92% with FSS and 70% without FSS.

REFERENCES

[1] Zaman, W., H. Ahmad, and H. Mehmood, "A miniaturized meandered printed monopole antenna for triband applications," *Microwave and Optical Technology Letters*, Vol. 60, No. 5, 1265–1271, May 2018.

[2] Zhi, R., M. Han, J. Bai, W. Wu, and G. Liu, "Miniature multiband antenna for WLAN and X-band satellite communication applications," *Progress In Electromagnetics Research Letters*, Vol. 75, 13–18, 2018.

[3] Cui, Y., L. Yang, B. Liu, and R. Li, "Multiband planar antenna for LTE/GSM/UMTS and WLAN/WiMAX handsets," *IET Microwaves, Antennas & Propagation*, Vol. 10, No. 5, 502–506, Apr. 2016.

[4] Osklang, P., C. Phongcharoenpanich, and P. Akkaraekthalin, "Triband compact printed antenna for 2.4/3.5/5 GHz WLAN/WiMAX applications," *International Journal of Antennas and Propagation*, Vol. 2019, Article ID 8094908, Aug. 2019.

[5] Ahmad, H., W. Zaman, S. Bashir, and M. Rahman, "Compact triband slotted printed monopole antenna for WLAN and WiMAX applications," *International Journal of RF and Microwave Computer-Aided Engineering*, Vol. 30, No. 1, e21986, Jan. 2020.

[6] Kunwar, A., A. K. Gautam, and B. K. Kanaujia, "Inverted L-slot triple-band antenna with defected ground structure for WLAN and WiMAX applications," *International Journal of Microwave and Wireless Technologies*, Vol. 9, No. 1, 191–196, 2015.

[7] Jing, J., J. Pang, H. Lin, Z. Qiu, and C. Liu, "A multiband compact low-profile planar antenna based on multiple resonant stubs," *Progress In Electromagnetics Research Letters*, Vol. 94, 1–7, 2020.

[8] Ran, X., Z. Yu, T. Xie, Y. Li, X. Wang, and P. Huang, "A novel dual-band binary branch fractal bionic antenna for mobile terminals," *International Journal of Antennas and Propagation*, Vol. 2020, Article ID 6109093, Jan. 2020.

[9] Wang, L., J. Yu, T. Xie, and K. Bi, "A novel multiband fractal antenna for wireless application," *International Journal of Antennas and Propagation*, Vol. 2021, Article ID 9926753, Jun. 2021.

[10] Verulkar, S. M., A. Khade, M. A. Trimukhe, and R. K. Gupta, "Dual band split ring monopole antenna structures for 5G and WLAN applications," *Progress In Electromagnetics Research C*, Vol. 122, 17–30, 2022.

[11] Din, I. U., S. Ullah, S. I. Naqvi, R. Ullah, S. Ullah, E. M. Ali, and M. Alibakhshikenari, "Improvement in the gain of UWB antenna for GPR applications by using frequency-selective surface," *International Journal of Antennas and Propagation*, Vol. 2022, 1–12, Article ID 2 002 552, 2022.

[12] Panda, P. K. and D. Ghosh, "Wideband and high gain tuning fork shaped monopole antenna using high impedance surface," *AEU — International Journal of Electronics and Communications*, Vol. 111, 152920, 2019.

[13] Abdelghany, M. A., M. F. A. Sree, A. Desai, and A. A. Ibrahim, "Gain improvement of a dual-band CPW monopole antenna for sub-6 GHz 5G applications using AMC structures," *Electronics*, Vol. 11, No. 14, 1–12, Jul. 2022.

[14] Shi, C., J. Zou, J. Gao, and C. Liu, "Gain enhancement of a dual-band antenna with the FSS," *Electronics*, Vol. 11, No. 18, 2882, Sep. 2022.

[15] Al-Gburi, A. J. A., I. M. Ibrahim, Z. Zakaria, M. K. Abdulhameed, and T. Saeidi, "Enhancing gain for UWB antennas using FSS: A systematic review," *Mathematics*, Vol. 9, No. 24, 3301, Dec. 2021.

[16] Aggarwal, I., S. Pandey, and M. R. Tripathy, "A high gain super wideband metamaterial based antenna," *Journal of Microwaves, Optoelectronics and Electromagnetic Applications*, Vol. 20, No. 2, 248–273, Jun. 2021.

[17] Kushwaha, N. and R. Kumar, "High gain UWB antenna using compact multilayer FSS," in *2014 IEEE International Microwave and RF Conference (IMaRC)*, 100–103, 2014.

[18] Ghosh, A., V. Kumar, G. Sen, and S. Das, "Gain enhancement of triple-band patch antenna by using triple-band artificial magnetic conductor," *IET Microwaves, Antennas & Propagation*, Vol. 12, No. 8, 1400–1406, Jul. 2018.

[19] Patil, S., R. Gupta, and S. Kharche, "Gain improvement of lower UWB monopole antenna using FSS layer," in *2017 International Conference on Nascent Technologies in Engineering (ICNTE)*,

1–5, Vashi, India, Jan. 2017.

[20] Nakmouche, M. F., A. M. Allam, D. E. Fawzy, and D.-B. Lin, "Development of a high gain FSS reflector backed monopole antenna using machine learning for 5G applications," *Progress In Electromagnetics Research M*, Vol. 105, 183–194, 2021.

[21] Liu, Q., H. Liu, W. He, and S. He, "A low-profile dual-band dual-polarized antenna with an AMC reflector for 5G communications," *IEEE Access*, Vol. 8, 24 072–24 080, 2020.

[22] Daira, S. E. I., M. Lashab, H. A. Berkani, M. Belattar, I. Gharbia, and R. A. Abd-Alhameed, "A curved single-layer FSS design for gain improvement of a compact size CPW-fed UWB monopole antenna," *Microwave and Optical Technology Letters*, Vol. 66, No. 1, 1–12, 2023.

[23] Mondir, A., M. A. Ennasar, L. Setti, and F. Mustapha, "Design, analysis, of high performance antennas for 5G communications analysis using WCIP," *Progress In Electromagnetics Research C*, Vol. 135, 211–226, 2023.

[24] Mondir, A., L. Setti, and R. E. Haffar, "Design, analysis, and modeling using WCIP method of novel microstrip patch antenna for THz applications," *Progress In Electromagnetics Research C*, Vol. 125, 67–82, 2022.

[25] Bembarka, A., L. Setti, A. Tribak, H. Tizyi, and M. E. Ouahabi, "A novel wideband beamforming antenna for 5G applications by eliminating the phase shifters and crossovers from the butler matrix," *Progress In Electromagnetics Research C*, Vol. 133, 51–63, 2023.

[26] Ray, K. P., "Design aspects of printed monopole antennas for ultra-wide band applications," *International Journal of Antennas and Propagation*, Vol. 2008, Article ID 713858, 2008.

[27] Kumar, G. and K. P. Ray, *Broadband Microstrip Antennas*, Artech House, 2003.